Cyclophilin A participates in the nuclear translocation of apoptosis-inducing factor in neurons after cerebral hypoxia-ischemia

Changlian Zhu,[1,3] Xiaoyang Wang,[2,3] Johanna Deinum,[4] Zhiheng Huang,[1,3] Jianfeng Gao,[1,3] Nazanine Modjtahedi,[5] Martha R. Neagu,[6,7] Michael Nilsson,[1] Peter S. Eriksson,[1] Henrik Hagberg,[2] Jeremy Luban,[6,7] Guido Kroemer,[5] and Klas Blomgren[1,8]

[1]Center for Brain Repair and Rehabilitation and [2]Perinatal Center, Institute of Neuroscience and Physiology, Göteborg University, 405 30 Göteborg, Sweden
[3]Department of Pediatrics, Third Affiliated Hospital of Zhengzhou University, Zhengzhou 450052, China
[4]AstraZeneca R&D, 431 83 Mölndal, Sweden
[5]Institut National de la Santé et de la Recherche Médicale, U848, Institute Gustave Roussy, 94805 Villejuif, France
[6]Institute for Research in Biomedicine, 6500 Bellinzona, Switzerland
[7]Department of Microbiology, Columbia University, New York, NY 10032
[8]Department of Pediatric Oncology, Queen Silvia Children's Hospital, 416 85 Göteborg, Sweden

Upon cerebral hypoxia-ischemia (HI), apoptosis-inducing factor (AIF) can move from mitochondria to nuclei, participate in chromatinolysis, and contribute to the execution of cell death. Previous work (Cande, C., N. Vahsen, I. Kouranti, E. Schmitt, E. Daugas, C. Spahr, J. Luban, R.T. Kroemer, F. Giordanetto, C. Garrido, et al. 2004. *Oncogene*. 23:1514–1521) performed in vitro suggests that AIF must interact with cyclophilin A (CypA) to form a proapoptotic DNA degradation complex. We addressed the question as to whether elimination of CypA may afford neuroprotection in vivo. 9-d-old wild-type (WT), CypA$^{+/-}$, or CypA$^{-/-}$ mice were subjected to unilateral cerebral HI. The infarct volume after HI was reduced by 47% ($P = 0.0089$) in CypA$^{-/-}$ mice compared with their WT littermates. Importantly, CypA$^{-/-}$ neurons failed to manifest the HI-induced nuclear translocation of AIF that was observed in WT neurons. Conversely, CypA accumulated within the nuclei of damaged neurons after HI, and this nuclear translocation of CypA was suppressed in AIF-deficient harlequin mice. Immunoprecipitation of AIF revealed coprecipitation of CypA, but only in injured, ischemic tissue. Surface plasmon resonance revealed direct molecular interactions between recombinant AIF and CypA. These data indicate that the lethal translocation of AIF to the nucleus requires interaction with CypA, suggesting a model in which two proteins that normally reside in separate cytoplasmic compartments acquire novel properties when moving together to the nucleus.

CORRESPONDENCE
Changlian Zhu:
changlian.zhu@neuro.gu.se

Cyclophilins constitute a family of phylogenetically conserved proteins found in prokaryotes as well as in humans. Cyclophilins have peptidyl-prolyl isomerase activity in vitro (1), indicating that they influence the conformation of proteins in cells, but their functions are largely unknown (2). The founding member of the cyclophilin family (15 members in humans), cyclophilin A (CypA), is an abundant, ubiquitously expressed protein originally discovered as an intracellular ligand of the immunosuppressive drug cyclosporin A (CsA) (3). CypA$^{-/-}$ embryonic stem cells grow normally and differentiate into hematopoietic precursor cells in vitro, indicating that CypA is not essential for mammalian cell viability (4). CypA$^{-/-}$ mice appear phenotypically normal, but with reduced fertility (unpublished data), and are resistant to immunosuppression by CsA (5). Immunosuppression is mediated by the CypA–CsA complex that inhibits calcineurin, a phosphatase crucial for T cell activation (6). CypA expression is particularly high in the brain, in neurons, where it is expressed mainly in the cytoplasm but also in the nucleus (7). Pioneering work by Montague et al. revealed that CypA possesses a latent, apoptosis-related DNase activity (8, 9). CypA has been

demonstrated to participate in excitotoxin-induced apoptosis (10) and to interact with a limited number of proteins, including dynein (11), the antioxidant protein Aop1 (12), the nuclear pore protein Nup358 (13), and apoptosis-inducing factor (AIF) (14).

CypA cooperates with AIF during apoptosis-associated chromatinolysis in vitro (14). Jurkat cells lacking CypA expression are relatively resistant to AIF-induced cell death (14). Similarly, disruption of the CypA homologue *CPR1* in yeast cells abrogated cell death induced by overexpression of AIF (15). In *Caenorhabditis elegans*, AIF (WAH-1) was found to interact with a cyclophilin within the molecular complex that mediates DNA degradation in apoptosis (16). In vitro, recombinant AIF and recombinant CypA together have a higher DNase activity than each of the proteins alone (14). Mutant CypA that lacks peptidyl-prolyl isomerase activity still cooperates with AIF to mediate chromatinolysis, and the proapoptotic cooperation of CypA and AIF was not inhibited by CsA (14), indicating that CsA is not a pharmacological tool to investigate the contribution of CypA and AIF to cell death.

We and others have demonstrated that AIF plays an important role in neuronal death after focal ischemia in the adult rodent brain (17–20) and after neonatal hypoxia-ischemia (HI) (21, 22). AIF translocates from mitochondria to the nuclei of dying neurons, and inhibition of this translocation (18, 19) or reduction of AIF expression through the harlequin (Hq) mutation is neuroprotective (17, 22). Thus, AIF contributes to the pathogenesis of adult stroke and perinatal asphyxia. The aim of this study was to explore the possible involvement of CypA in brain injury induced by neonatal HI. We demonstrate that CypA and AIF functionally and physically interact in vivo in neonatal HI and in vitro using surface plasmon resonance, and that the CypA knockout confers resistance against HI-induced neuronal loss.

RESULTS AND DISCUSSION

Impact of CypA deficiency on brain injury after HI

Brain injury was significantly reduced at 72 h after HI in all four examined brain regions of $CypA^{-/-}$ mice compared with WT and $CypA^{+/-}$ littermates, as evaluated by neuropathological scores, but there were no significant differences between the WT and $CypA^{+/-}$ groups (Fig. 1, A and B). The total infarct volume was reduced by 46.7% ($P = 0.0089$) in $CypA^{-/-}$ mice (12.72 ± 3.19 mm^3; $n = 19$) compared with WT mice (23.87 ± 3.22 mm^3; $n = 25$; Fig. 1 C). The infarct volume was reduced by 13.6% in $CypA^{+/-}$ mice (20.62 ± 2.25 mm^3; $n = 27$), which was not significantly different from WT mice (Fig. 1 C). The total tissue loss was reduced by 33.8% in $CypA^{-/-}$ mice (28.37 ± 3.87 mm^3) compared with WT mice (42.86 ± 3.50 mm^3) and by 29.9% compared with $CypA^{+/-}$ mice (40.48 ± 2.21 mm^3; Fig. 1 D). This is the first in vivo study showing that CypA deficiency is neuroprotective. The degree of protection against HI-induced infarction is impressive (almost 50%), which is probably close to the maximum that can be attained in this animal model, considering that the infarct cores are beyond rescue and that neuroprotective strategies can salvage only penumbral areas. The degree of protection is in the same range as that observed for mice with relative AIF deficiency, the so-called Hq mice (22). A functional connection between AIF and CypA was recently found in vitro, demonstrating that AIF and CypA bind to each other upon induction of apoptosis in Jurkat cells and that the AIF–CypA complex, but neither of the individual constituents alone, could produce nonspecific, large-scale DNA degradation (14).

We next examined the mechanisms underlying the neuroprotective effect of CypA deficiency. No CypA protein was detected in $CypA^{-/-}$ mice, and the level of CypA protein was reduced ~50% in $CypA^{+/-}$ compared with WT mice, as judged by immunoblotting (Fig. 2 A). $CypA^{-/-}$ mice were not phenotypically different from WT mice, and the brain morphology was not different between the two genotypes (unpublished data). The expression of neither the mitochondrial proapoptotic proteins AIF, Cyt c, and Smac, nor the mitochondrial oxidative stress–related proteins SOD2 and Trx2, were changed in $CypA^{-/-}$ nonischemic mice compared with $CypA^{+/-}$ or WT mice (Fig. 2 A). 24 h after HI, the mitochondrial proteins AIF, cyt c, Smac, and SOD2 were reduced in the mitochondrial fraction of the ipsilateral cortex compared with the contralateral side, but the decrease was the same in WT and $CypA^{-/-}$ mice (Fig. 2 B). Thus, CypA deficiency does not inhibit the mitochondrial release of cell-death effectors. The nonmitochondrial oxidative stress–related proteins catalase and SOD1 were not changed at 24 h after HI (Fig. 2 C). Hsp70, a chaperone known to counteract the proapoptotic effects of AIF, was not different between WT and $CypA^{-/-}$ mice (Fig. 2 C). The fodrin breakdown products generated by calpain (145/150 kD) and caspase-3 activation (120 kD) were not different between WT and $CypA^{-/-}$ mice, nor was the calpain-induced degradation of Na^+/Ca^{2+} exchanger 1 (NCX1; Fig. 2 C) (23). Accordingly, the capacity to cleave caspase-3 (Fig. 2 D) and caspase-9 (not depicted) peptide substrates was not different in WT compared with $CypA^{-/-}$ mice in homogenates of normal control or postischemic cortical tissue 24 h after HI. Thus, CypA deficiency had no effect on the HI-induced activation of proteases, including calpains and caspases. The levels of AIF, HSP70, or oxidative stress–related proteins were not different between WT and $CypA^{-/-}$ mice and, hence, cannot explain the AIF-related, protective effects observed in $CypA^{-/-}$ mice. The AIF deficiency in Hq mice reduces the antioxidant defense of neurons, thereby enhancing their susceptibility to oxidative stress (22, 24), but we could not find any indications of altered levels of antioxidative stress–related proteins in $CypA^{-/-}$ mice. Interestingly, caspase-3– and caspase-9–like activities increased after HI to a similar level in WT and $CypA^{-/-}$ mice despite the fact that WT mice developed brain infarcts that were almost twice as large as those from $CypA^{-/-}$ mice. This is in accordance with our previous finding that the neuroprotection afforded by the Hq mutation does not correlate with reduced caspase

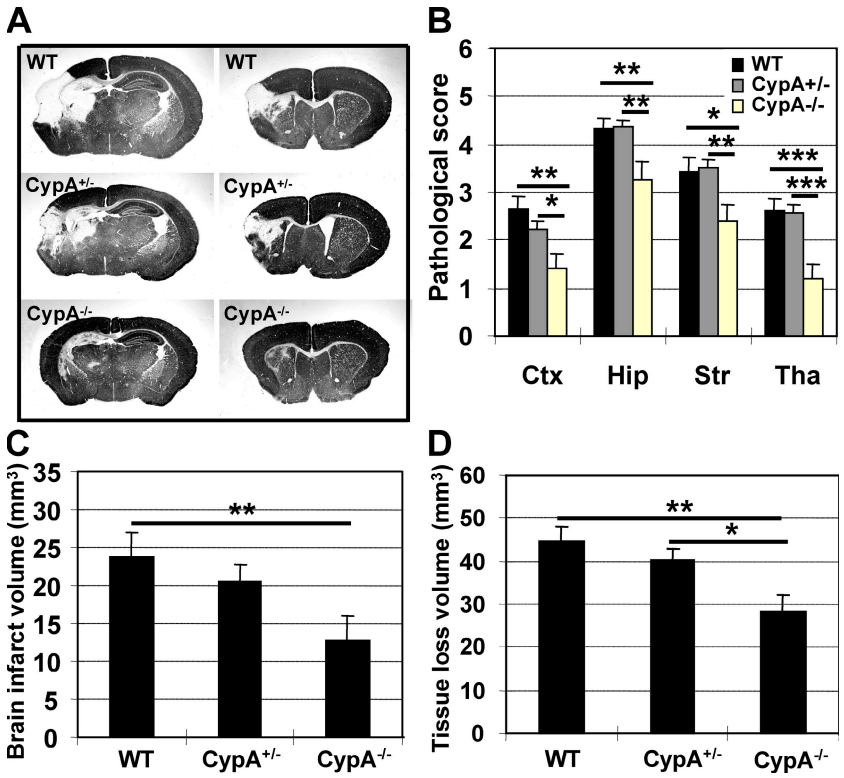

Figure 1. Neuroprotective effects of CypA deficiency in a model of neonatal HI. (A) Representative MAP2 stainings obtained 72 h after HI at the dorsal hippocampus (left) and striatum (right) levels are shown for WT, CypA$^{+/-}$, and CypA$^{-/-}$ brains. Brain injury was evident in the cortex, striatum, hippocampus, and thalamus, and was more pronounced in WT than in CypA$^{-/-}$ mice. (B) Neuropathological scores in the cortex (Ctx), hippocampus (Hip), striatum (Str), and thalamus (Tha). (C) The total infarct volume was reduced by 46.7% in CypA$^{-/-}$ ($n = 19$; $P = 0.0089$) as compared with WT mice ($n = 25$) and by 38.3% as compared with CypA$^{+/-}$ mice ($n = 27$; NS). (D) The volume of total tissue loss was measured 72 h after HI, as described in Materials and methods. The CypA$^{-/-}$ mice displayed 33.8% less tissue loss than the WT mice ($P = 0.0025$) and 29.9% less than the CypA$^{+/-}$ mice ($P = 0.0113$). Data presented represent the mean ± SEM. *, $P < 0.05$; **, $P < 0.01$; ***, $P < 0.001$.

activation (22), yet it stands in contrast with the notion that caspases, particularly caspase-3, are critically important for the development of brain injury in the immature brain (22, 25). This may suggest that caspase-independent apoptosis-related cell-death mechanisms are particularly important in determining cell fate after brain injury. Clearly, the CypA–AIF interaction plays a greater role in pathological neuronal death than in normal, developmentally regulated programmed cell death, because CypA$^{-/-}$ mice do not display any dysmorphic or teratogenic features (5).

Functional and physical interaction of CypA and AIF after HI in neurons

In healthy neurons, CypA is localized both in the cytoplasm and nuclei, whereas AIF is confined to mitochondria. In WT mice, nuclear translocation of both AIF and CypA was evident in injured (pyknotic) neurons after HI, as judged by immunofluorescence stainings (Fig. 3 A). In a separate experiment, 93% of the cells with nuclear AIF were identified as neurons (NeuN positive; unpublished data). In CypA$^{-/-}$ mice, nuclear translocation of AIF could be detected in injured neurons, but the signal was very weak (Fig. 3 B) compared with WT mice (Fig. 3 A). Conversely, in AIF-deficient mice carrying the Hq mutation, CypA staining in the nucleus was reduced (Fig. 3 C). These data suggest that CypA is required for the optimal nuclear translocation of AIF in damaged neurons and, vice versa, that AIF is needed for the nuclear translocation of CypA after HI. Accordingly, CypA coimmunoprecipitated with AIF in the ipsilateral, ischemic hemisphere but not in normal control tissue (Fig. 4 A). This suggested a direct physical interaction between AIF and CypA, and this was confirmed using surface plasmon resonance (Biacore). Recombinant AIF was captured by an antibody immobilized to the sensor surface, and recombinant CypA bound to and was released from the captured AIF with an apparent dissociation constant (K_d) of 1 μM (Fig. 4 B). Thus, direct physical interaction between AIF and CypA was demonstrated in vitro and in vivo after HI.

Double labeling of AIF and the DNA strand break marker Tdt-mediated dUTP-biotin nick-end labeling (TUNEL) revealed intense nuclear AIF immunoreactivity in TUNEL-positive cells from WT mice (Fig. 5 A) but reduced nuclear AIF immunoreactivity in TUNEL-positive CypA$^{-/-}$ neurons (Fig. 5 B). Similarly, TUNEL-positive nuclei in WT mice displayed strong CypA immunoreactivity (Fig. 5 C), whereas AIF-deficient Hq mutant mice displayed weak CypA

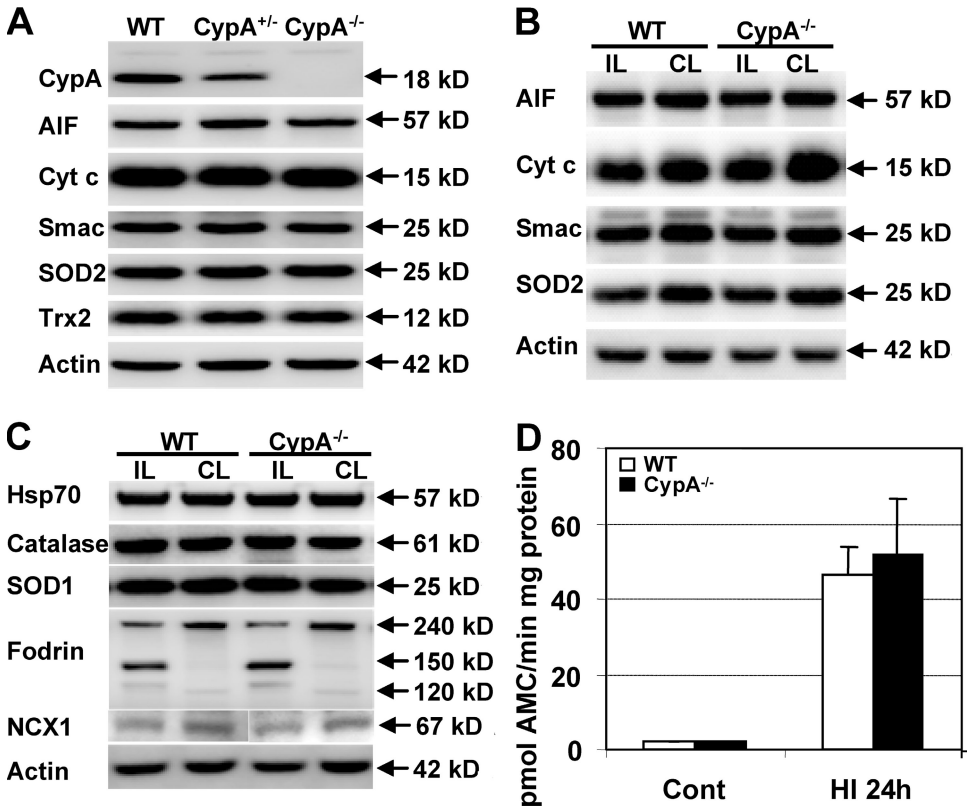

Figure 2. Apoptosis- and oxidative stress–related proteins under physiological and pathological conditions in WT and CypA$^{-/-}$ mice. (A) Immunoblots of CypA and selected apoptosis-related (AIF, cyt c, and Smac) and oxidative stress–related (SOD2 and Trx2) proteins in homogenates from nonischemic WT, CypA$^{+/-}$, and CypA$^{-/-}$ brains ($n = 5$ per group). CypA was not detectable in CypA$^{-/-}$ brains and was decreased ~50% in CypA$^{+/-}$ mice. There were no detectable differences in AIF, Cyt c, Smac, SOD2, or Trx2 ($P > 0.43$). Actin was used as a loading control. (B) Immunoblots of mitochondrial proteins in the ipsilateral (IL; ischemic, injured) and contralateral (CL; hypoxic, uninjured) cortex of WT and CypA$^{-/-}$ mice 24 h after HI. AIF, Cyt c, Smac, and SOD2 were decreased in the ipsilateral hemisphere, but the decrease was not different between WT and CypA$^{-/-}$ mice ($P > 0.31$). (C) Immunoblots of homogenates from the ipsilateral and contralateral cortex of WT and CypA$^{-/-}$ mice 24 h after HI. There were no differences in the levels of HSP70, catalase, or SOD1, neither after HI nor between genotypes ($P > 0.25$). The 240-kD cytoskeletal protein fodrin was cleaved into 145/150-kD calpain-related fragments and a 120-kD caspase-3–related fragment in the ipsilateral hemisphere, but the extent of cleavage was not significantly difference between WT and CypA$^{-/-}$ mice ($P = 0.49$). Calpain-induced cleavage of NCX1 was not different between genotypes ($P = 0.42$). The white line indicates that intervening lanes have been spliced out. (D) Caspase-3–like activity (DEVD cleavage) in the cortex from WT and CypA$^{-/-}$ mice in nonischemic control tissue (Cont) ($P = 0.12$) and ischemic tissue 24 h after HI ($P = 0.75$) was not significantly different between WT and CypA$^{-/-}$ mice, despite the difference in infarct volume ($n = 6$ per group). Data represent the mean ± SEM.

immunoreactivity in TUNEL-positive nuclei (Fig. 5 D). The number of TUNEL-positive nuclei also positive for AIF or CypA was determined in WT, CypA$^{-/-}$, and Hq mice 24 h after HI within the penumbra. Approximately 253 TUNEL-positive neurons per mm^2 displayed nuclear AIF staining in WT mice, whereas in CypA$^{-/-}$ mice the number of TUNEL-positive cells with nuclear AIF staining was reduced by 90.7% ($P < 0.0001$; Fig. 5 E). Similarly, the number of TUNEL/CypA double-positive neurons decreased by 79.4% in Hq compared with WT mice ($P < 0.0004$; Fig. 5 F). Furthermore, the total number of TUNEL-positive cells after HI was reduced to a greater extent in CypA$^{-/-}$ and Hq mice than would be expected from the degree of protection (Fig. 5, E and F).

These findings provide a possible mechanism whereby AIF could exert its proapoptotic effects when released from mitochondria. We anticipate that under normal conditions, AIF and CypA reside in separate cellular compartments, with AIF in the mitochondrial intermembrane space and CypA in the cytoplasm and nuclei. Thus, both proteins would be prevented from interacting under normal conditions but can bind to each other upon induction of cell-death signaling and mitochondrial membrane permeabilization. The domain of the AIF protein that interacts with CypA is separate from its HSP70 interaction domain and from its DNA binding sites (14). The domain of CypA that binds to AIF is separate from its catalytic domain and its binding site for CsA (14). Previous studies could not conclusively determine in which subcellular compartment the AIF–CypA interaction occurred, but it was assumed that AIF underwent electrostatic interaction with DNA (26) and then tethered CypA to chromatin (14). Our data suggest that the CypA–AIF interaction occurs before or when nuclear translocation begins, in the cytosol.

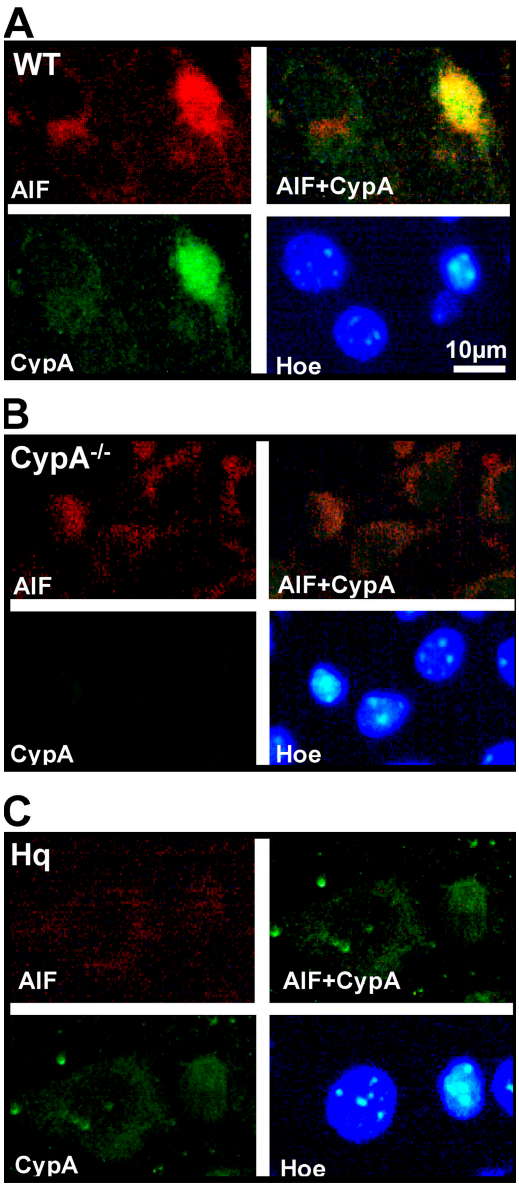

Figure 3. Nuclear translocation of AIF was impaired in the absence of CypA and vice versa. (A) Immunofluorescent labeling of AIF (red), CypA (green), and chromatin (HOECHST 33342; blue) 3 h after HI in WT type mice showing both strong AIF and CypA nuclear staining in an injured neuron, as judged by the condensed nuclear morphology. (B) Labeling, as in A, in $CypA^{-/-}$ mice showing very weak nuclear AIF staining in injured neurons. (C) Labeling, as in A, in AIF-deficient Hq mice showing very weak CypA staining in injured neurons compared with WT type mice. Bar, 10 μm.

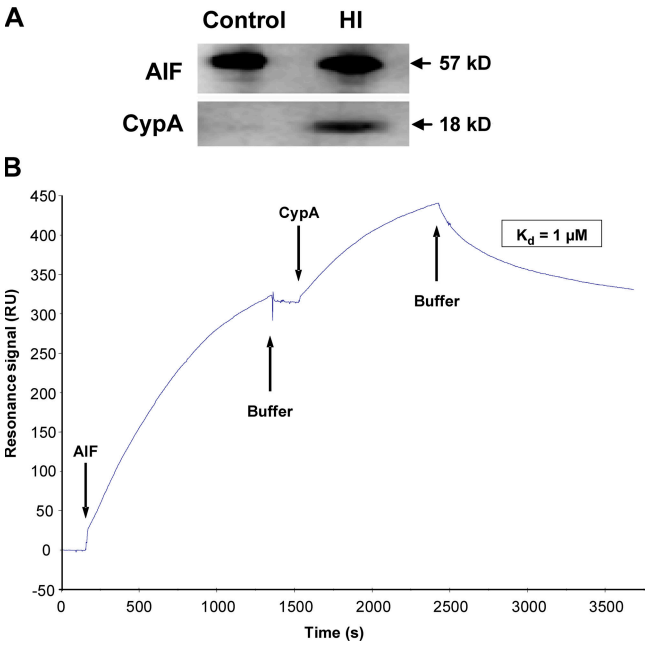

Figure 4. Physical interaction between CypA and AIF after HI in vivo and in vitro. (A) Coimmunoprecipitation of CypA and AIF in ischemic but not in nonischemic brain tissue. Immunoprecipitation of AIF in nonischemic control and ipsilateral, HI cortex homogenates 3 h after HI. (B) Surface plasmon resonance measurement of the CypA–AIF interaction. The curve demonstrates the net resonance signal in RU obtained by subtracting the reference channel from the experimental channel. Recombinant AIF protein was captured by an immobilized antibody raised against AIF, resulting in a 320-RU rise. Subsequent injection of CypA resulted in a 123-RU rise, indicating CypA binding to AIF. This binding was reversible, because CypA dissociated upon change to buffer flow until the initial plateau value was reached. The dissociation constant was calculated to ~1 μM. Repeated injections of CypA resulted in the same association and dissociation phases as found in the first injection.

This is based on the observations that nuclear translocation of AIF was reduced (by ~90%) in injured neurons in $CypA^{-/-}$ mice and, conversely, that CypA translocation to nuclei was reduced (by ~80%) in AIF-deficient Hq mice. Conclusively, these data suggest that CypA is required for efficient nuclear translocation of AIF in damaged neurons and, conversely, that AIF is needed for the nuclear translocation of CypA after HI. This suggests a direct physical interaction between AIF and CypA, and this was confirmed using coimmunoprecipitation and surface plasmon resonance technology. Presumably, the physical interaction between CypA and AIF facilitates nuclear translocation of the two proteins as a complex.

In summary, this is the first study to our knowledge demonstrating that elimination of CypA affords neuroprotection in vivo. It has been demonstrated in vitro that AIF and CypA cooperate in caspase-independent apoptosis-related DNA fragmentation. Our in vivo data support and extend this cooperative mechanism. Until now, the only possibility to inhibit the lethal action of AIF in HI was to prevent mitochondrial membrane permeabilization, e.g., by targeting the antiapoptotic Bcl-2 family protein Bcl-XL to neurons (20), or to prevent the translocation of AIF to the nucleus by overexpressing transgenic HSP70 in neurons (18). Our data demonstrate yet another possible strategy for inhibiting the action of AIF, namely by generating pharmacological inhibitors of the CypA–AIF interaction. This strategy constitutes a challenging endeavor for future research.

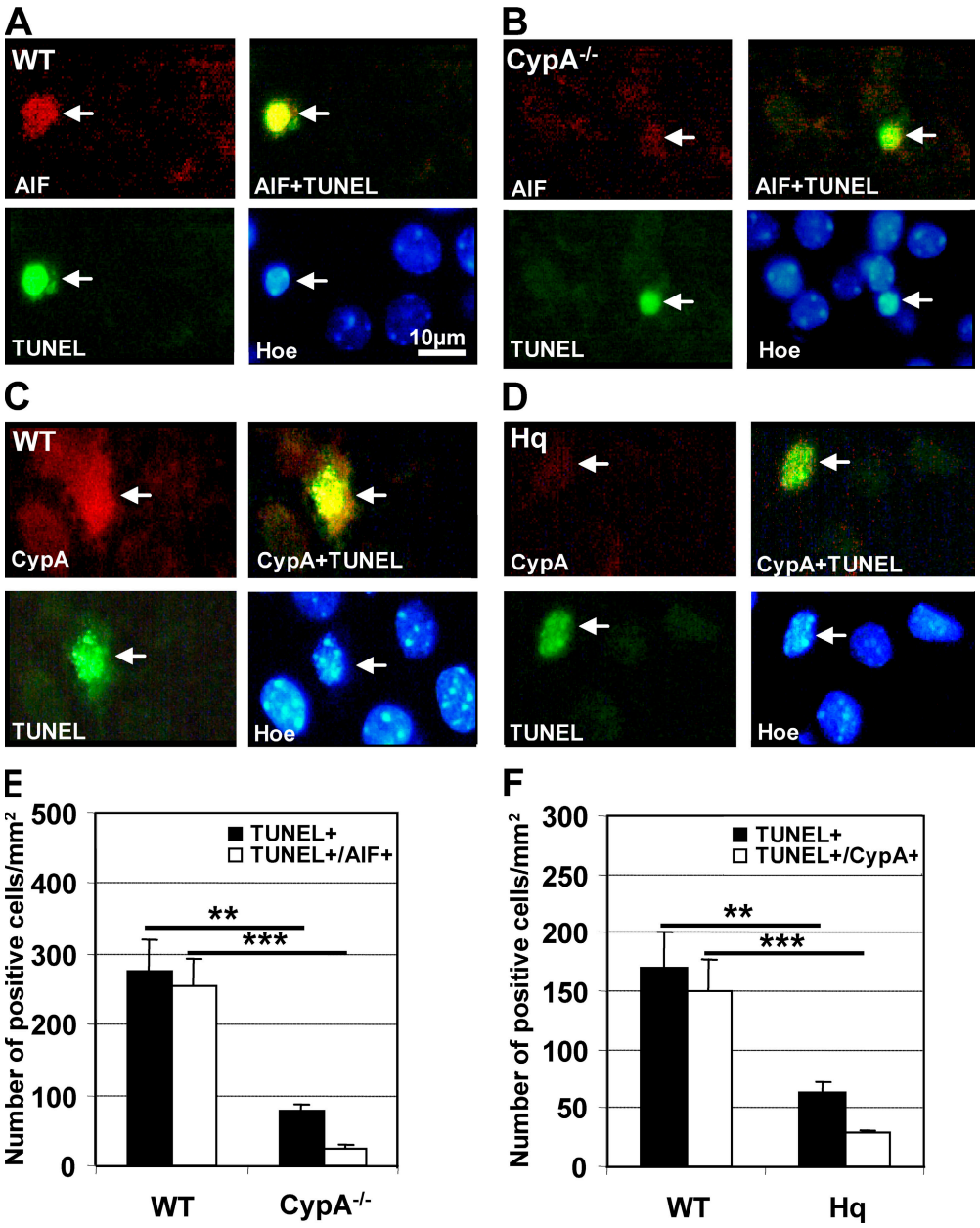

Figure 5. Obligate cotranslocation of AIF and CypA into the nuclei of damaged neurons. DNA strand breaks in the cortex 3 or 24 h after HI were identified using TUNEL labeling (green) and correlated with AIF (A and B, red) or CypA (C and D, red) immunolabeling. Nuclear morphology was evaluated with HOECHST 33342 (blue). (A) A TUNEL-positive neuron (arrow, green) displaying strong nuclear AIF staining (red) and condensed chromatin (blue), unlike the noninjured, TUNEL-negative neurons. (B) In CypA$^{-/-}$ mice nuclear AIF staining (arrow, red) was weak in the TUNEL-positive neurons (green) with condensed chromatin (blue). (C) A TUNEL-positive neuron (arrow, green) displaying strong nuclear CypA staining (red) and condensed chromatin (blue), unlike the noninjured, TUNEL-negative neurons. Bar, 10 μm. (D) In AIF-deficient Hq mice, TUNEL-positive neurons (arrow, green) with condensed nuclear morphology (blue) displayed weak nuclear CypA staining (red). (E) Quantification of TUNEL-positive cells with AIF-positive nuclei in the cortical penumbra 24 h after HI. WT brains contained 276 ± 44 TUNEL-positive neurons per mm^2 24 h after HI, whereas CypA$^{-/-}$ mice displayed only 78 ± 10 neurons per mm^2 (**, $P = 0.0003$). The density of cells positive for both TUNEL and AIF was 253 ± 40 cells per mm^2 in WT and 23 ± 6 cells per mm^2 in CypA$^{-/-}$ mice ($n = 6$ per group; ***, $P < 0.0001$). (F) Quantification of TUNEL-positive cells with CypA-positive nuclei in the cortical penumbra 24 h after HI. WT mice exhibited 170 ± 31 TUNEL-positive neurons per mm^2 24 h after HI, whereas this value amounted to 64 ± 8 neurons per mm^2 in Hq mice (**, $P = 0.0011$). The density of cells positive for both TUNEL and CypA was 150 ± 28 cells per mm^2 in WT and 29 ± 2 cells per mm^2 in Hq mice ($n = 6$ per group; ***, $P < 0.0004$).

MATERIALS AND METHODS

HI. CypA$^{-/-}$ mice (5) and their heterozygous (CypA$^{+/-}$) or WT littermates of either sex were subjected to unilateral HI on postnatal day 9 (P9), essentially according to the Rice-Vannucci model (25). AIF-deficient Hq male mice (24) and their WT littermates were subjected to the same procedure. In brief, mice were anesthetized with isoflurane, and the left common carotid artery was cut between double ligatures of prolene sutures. After surgery, the pups were allowed to recover for 1–1.5 h with the dam and were then placed in a chamber perfused with a humidified gas mixture (10% oxygen in nitrogen) for 45 min. After hypoxic exposure, the pups were returned to their biological dams until they were killed. Interesting differences between neuronal mechanisms of injury in neonatal male and female brains have been observed, including more pronounced nuclear translocation of AIF during early reperfusion ($P < 0.05$) (27). We did not find any significant differences between males and females regarding the injury observed or the frequency of neurons with nuclear AIF (unpublished data), as expected at the particular time points of evaluation shown in the figures (22, 27), so both male and female CypA$^{-/-}$, CypA$^{+/-}$, and WT pups were included in this study. All animal experimental protocols were approved by the Göteborg committee of the Swedish Animal Welfare Agency (application nos. 94–2003 and 184–2003).

Genotyping. Hq genotyping was previously described (22). For CypA mice genotyping, the following primers were used: CypA common, 5′-GCAGTTGTGATTGATCCAGGTCCG-3′; CypA WT, 5′-CACCCTGGAGCACCACTGCCCACC-3′; and CypA mutant, 5′-CCTGATCGACAAGACCGGCTTCC-3′. CypA$^{-/-}$ mice were identified by the presence of a single 520-bp DNA band. WT mice were identified by a single 200-bp product. CypA$^{+/-}$ mice were identified by the presence of both bands.

Immunohistochemistry. Mice were deeply anesthetized with 50 mg/ml phenobarbital and perfusion fixed with 5% formaldehyde. Brains were dehydrated with xylene and graded ethanol, paraffin embedded, and serial cut into 5-μm coronal sections. Sections were deparaffinized, and antigen retrieval was performed by boiling them in 10 mM sodium citrate buffer (pH 6) for 10 min. Nonspecific binding was blocked for 30 min with 4% horse serum in PBS. 4 μg/ml anti–microtubule-associated protein 2 (anti-MAP2; clone HM-2; Sigma-Aldrich) was incubated for 60 min at 20°C, followed by another 60 min with 2 μg/ml of a biotinylated horse anti–mouse IgG diluted in PBS. Visualization was performed using Vectastain ABC Elite (Vector Laboratories).

Immunofluorescence staining. Antigen retrieval was performed as described in the previous section. Nonspecific binding was blocked for 30 min with 4% donkey serum in PBS. 2 μg/ml anti-AIF (goat polyclonal antibody; Santa Cruz Biotechnology, Inc.) and anti-CypA (1:400; rabbit polyclonal antibody; BIOMOL Research Laboratories, Inc.) or anti-NeuN (1:500; clone HM-2; Sigma-Aldrich) in PBS were incubated overnight at 4°C. After washing with PBS, sections were incubated with donkey anti–goat 546 (1:150) and donkey anti–rabbit 488 (1:150) or donkey anti–mouse 488 (1:150) in PBS for 2 h at room temperature, and were subsequently placed in HOECHST 33342 (Invitrogen) at 1 μg/ml in PBS for 10 min at 20°C with gentle agitation, washed, and mounted using Vectashield mounting medium. For TUNEL and AIF or CypA double labeling, sections were incubated with 3% bovine serum albumin in 0.1 M Tris-HCl (pH 7.5) for 30 min, followed by 50 μl of TUNEL reaction mixture (Roche) on each sample for 60 min at 37°C in a moist chamber. After washing, the sections were blocked with 4% donkey serum and incubated either with anti-AIF or anti-CypA, as described. Secondary donkey anti–goat 546 (for AIF) or donkey anti–rabbit 546 (for CypA; Invitrogen) was used, and staining with HOECHST 33342 was performed as described.

Western blot analysis. Homogenates and cellular fractions from parietal cortex (harboring both injured and intact tissue) were prepared as previously described (22). The samples were run on 4–12% NuPAGE Bis-Tris gels (Novex) and transferred to reinforced nitrocellulose membranes (Schleicher & Schuell). The following primary antibodies were used: anti-actin (1:200; Sigma-Aldrich), 0.2 μg/ml anti-AIF, 1 μg/ml anticatalase (clone 11A1; Lab Frontier), anti-CypA (1:4,000), anti–cytochrome c (1:500; clone 7H8.2C12; BD Biosciences), 0.2 μg/ml antifodrin (clone AA6; BIOMOL Research Laboratories, Inc.), 0.5 μg/ml anti–heat-shock protein 70 (HSP 70; Santa Cruz Biotechnology, Inc.), 0.7 μg/ml anti-Smac (Santa Cruz Biotechnology, Inc.), 0.5 μg/ml anti–superoxide dismutase I (Cu/Zn-SOD/SOD1; Lab Frontier), 0.5 μg/ml anti–superoxide dismutase II (Mn-SOD/SOD2; clone 2A1; Lab Frontier), 1 μg/ml anti–thioredoxin 2 (Trx2; Lab Frontier), and 0.25 μg/ml anti-NCX1 (1:800; Santa Cruz Biotechnology, Inc.). Peroxidase-labeled secondary antibodies (1:2,000 goat anti–rabbit, 1:2,000 horse anti–goat, or 1:4,000 horse anti–mouse) were obtained from Vector Laboratories. Immunoreactive species were visualized using a substrate (Super Signal Western Dura; Pierce Chemical Co.) and a cooled CCD camera (LAS 3000; Fuji).

Caspase activity assays. 25-μl homogenate samples were mixed with 75 μl of extraction buffer, as previously described (28). Cleavage of Ac-DEVD-AMC (for caspase-3; Peptide Institute) was measured with an excitation wavelength of 380 nm and an emission wavelength of 460 nm and expressed as picomoles of AMC released per milligran of protein per minute. Cleavage of Ac-LEHD-AFC (for caspase-9; Enzyme System Products) was measured as for the AFC conjugates, but with an excitation wavelength of 400 nm and an emission wavelength of 505 nm, and expressed as picomoles of AMC released per milligran of protein per minute.

Injury evaluation. Brain injury was evaluated by neuropathological scoring as well as calculating infarct volume and the volume of total tissue loss at 72 h after HI (22). Sections were stained for MAP2 and scored by an observer blinded to the genotype of the mice. The total score (0–22) was the sum of the scores for all four regions (cortex, hippocampus, striatum, and thalamus) (29). The infarct areas (MAP2 negative) were measured using Micro-Imaging (Olympus). Total tissue loss was calculated as the MAP2-positive areas in the contralateral hemisphere minus the MAP2-positive areas in the ipsilateral hemisphere (29).

Immunoprecipitation. AIF was immunoprecipitated from control tissue or ipsilateral (ischemic) hemispheres 3 h after HI. Homogenate samples containing equal amounts of protein were precleaned with goat IgG and PANSORBIN cells (Calbiochem), followed by the addition of 1 μg anti-AIF (sc-9416; Santa Cruz Biotechnology, Inc.) and incubation overnight at 4°C. Immune complexes were sequestered through the addition of 50 μl of Pansorbin cells and incubation for an additional 2 h at 20°C. The resulting immobilized immune complexes were pelleted by centrifugation at 3,000 *g* for 5 min at 4°C and washed four times with 0.5 ml homogenizing buffer. The bound proteins were eluted by heating in NuPAGE LDS 4× sample buffer for 10 min. Immunoprecipitated proteins were subjected to immunoblotting and examined for AIF and CypA immunoreactivity.

Surface plasmon resonance. CypA interaction with AIF was explored with the surface plasmon resonance technique, using a BIACORE 3000 (Biacore AB). The Biacore HBS-EP buffer (10 mM Hepes, 150 mM NaCl, 3.4 mM EDTA, and 0.01% polysorbate P20, pH 7.4) was used as a running buffer at 5 μl/min and 25°C in all experiments. A goat polyclonal anti-AIF (0.05 μg/ml in 10 mM sodium acetate, pH 5) was amine-coupled to a CM4 sensor chip (Biacore AB), according to the standard procedure recommended, to a response of 6,000 resonance units (RU). 100 μl, 0.2 μg/ml AIF protein (30) in running buffer with 1 mM nicotinamide adenine dinucleotide phosphate (NADPH) was passed over the surface, resulting in binding of 320 RU (Fig. 4). Captured AIF was apparently tightly bound to the antibody surface, because the dissociation rate was very slow. 75 μl, 25 nM CypA protein (Affinity BioReagents, Inc.) in running buffer with 1 mM NADPH was injected. After association of CypA to 123 RU, CypA dissociated upon change to buffer flow until the initial plateau value for the

bound AIF was reached. A dissociation equilibrium constant for AIF and CypA of ~1 μM was determined using BIAeval software (Biacore AB), assuming mass transport.

Statistics. All data were expressed as mean ± SEM. The Student's *t* test was used when comparing two groups, whereas analysis of variance with Fisher's post-hoc test was used when comparing three or more groups. The Mann-Whitney U test was used when comparing the ratios of double-positive cells.

This work was supported by the Swedish Child Cancer Foundation (K. Blomgren), Swedish governmental grants to scientists working in health care (to K. Blomgren and H. Hagberg), the Swedish Research Council (H. Hagberg and K. Blomgren), grant 30470598 from the National Natural Science Foundation of China (to C. Zhu), Trans-Death European Union and Agence Nationale pour la Recherche grants (to G. Kroemer), grant RO1AI59159 from the National Institutes of Health (to J. Luban), the King Gustav V Jubilee Clinic Research Foundation (JK-fonden), the Wilhelm and Martina Lundgren Foundation, the Frimurare Barnhus Foundation, the Göteborg Medical Society, and the Swedish Society of Medicine.

The authors have no conflicting financial interests.

Submitted: 25 January 2007
Accepted: 22 June 2007

REFERENCES

1. Fischer, G., B. Wittmann-Liebold, K. Lang, T. Kiefhaber, and F.X. Schmid. 1989. Cyclophilin and peptidyl-prolyl cis-trans isomerase are probably identical proteins. *Nature*. 337:476–478.
2. Schiene, C., and G. Fischer. 2000. Enzymes that catalyse the restructuring of proteins. *Curr. Opin. Struct. Biol*. 10:40–45.
3. Handschumacher, R.E., M.W. Harding, J. Rice, R.J. Drugge, and D.W. Speicher. 1984. Cyclophilin: a specific cytosolic binding protein for cyclosporin A. *Science*. 226:544–547.
4. Colgan, J., M. Asmal, and J. Luban. 2000. Isolation, characterization and targeted disruption of mouse ppia: cyclophilin A is not essential for mammalian cell viability. *Genomics*. 68:167–178.
5. Colgan, J., M. Asmal, B. Yu, and J. Luban. 2005. Cyclophilin A-deficient mice are resistant to immunosuppression by cyclosporine. *J. Immunol*. 174:6030–6038.
6. Liu, J., J.D. Farmer Jr., W.S. Lane, J. Friedman, I. Weissman, and S.L. Schreiber. 1991. Calcineurin is a common target of cyclophilin-cyclosporin A and FKBP-FK506 complexes. *Cell*. 66:807–815.
7. Goldner, F.M., and J.W. Patrick. 1996. Neuronal localization of the cyclophilin A protein in the adult rat brain. *J. Comp. Neurol*. 372: 283–293.
8. Montague, J.W., M.L. Gaido, C. Frye, and J.A. Cidlowski. 1994. A calcium-dependent nuclease from apoptotic rat thymocytes is homologous with cyclophilin. Recombinant cyclophilins A, B, and C have nuclease activity. *J. Biol. Chem*. 269:18877–18880.
9. Montague, J.W., F.M. Hughes Jr., and J.A. Cidlowski. 1997. Native recombinant cyclophilins A, B, and C degrade DNA independently of peptidylprolyl cis-trans-isomerase activity. Potential roles of cyclophilins in apoptosis. *J. Biol. Chem*. 272:6677–6684.
10. Capano, M., S. Virji, and M. Crompton. 2002. Cyclophilin-A is involved in excitotoxin-induced caspase activation in rat neuronal B50 cells. *Biochem. J*. 363:29–36.
11. Galigniana, M.D., Y. Morishima, P.A. Gallay, and W.B. Pratt. 2004. Cyclophilin-A is bound through its peptidylprolyl isomerase domain to the cytoplasmic dynein motor protein complex. *J. Biol. Chem*. 279:55754–55759.
12. Jaschke, A., H. Mi, and M. Tropschug. 1998. Human T cell cyclophilin18 binds to thiol-specific antioxidant protein Aop1 and stimulates its activity. *J. Mol. Biol*. 277:763–769.
13. Wu, J., M.J. Matunis, D. Kraemer, G. Blobel, and E. Coutavas. 1995. Nup358, a cytoplasmically exposed nucleoporin with peptide repeats, Ran-GTP binding sites, zinc fingers, a cyclophilin A homologous domain, and a leucine-rich region. *J. Biol. Chem*. 270:14209–14213.
14. Cande, C., N. Vahsen, I. Kouranti, E. Schmitt, E. Daugas, C. Spahr, J. Luban, R.T. Kroemer, F. Giordanetto, C. Garrido, et al. 2004. AIF and cyclophilin A cooperate in apoptosis-associated chromatinolysis. *Oncogene*. 23:1514–1521.
15. Wissing, S., P. Ludovico, E. Herker, S. Buttner, S.M. Engelhardt, T. Decker, A. Link, A. Proksch, F. Rodrigues, M. Corte-Real, et al. 2004. An AIF orthologue regulates apoptosis in yeast. *J. Cell Biol*. 166:969–974.
16. Parrish, J.Z., and D. Xue. 2003. Functional genomic analysis of apoptotic DNA degradation in *C. elegans*. *Mol. Cell*. 11:987–996.
17. Culmsee, C., C. Zhu, S. Landshamer, B. Becattini, E. Wagner, M. Pellecchia, K. Blomgren, and N. Plesnila. 2005. Apoptosis-inducing factor triggered by poly(ADP-ribose) polymerase and Bid mediates neuronal cell death after oxygen-glucose deprivation and focal cerebral ischemia. *J. Neurosci*. 25:10262–10272.
18. Matsumori, Y., S.M. Hong, K. Aoyama, Y. Fan, T. Kayama, R.A. Sheldon, Z.S. Vexler, D.M. Ferriero, P.R. Weinstein, and J. Liu. 2005. Hsp70 overexpression sequesters AIF and reduces neonatal hypoxic/ischemic brain injury. *J. Cereb. Blood Flow Metab*. 25:899–910.
19. Niimura, M., N. Takagi, K. Takagi, R. Mizutani, N. Ishihara, K. Matsumoto, H. Funakoshi, T. Nakamura, and S. Takeo. 2006. Prevention of apoptosis-inducing factor translocation is a possible mechanism for protective effects of hepatocyte growth factor against neuronal cell death in the hippocampus after transient forebrain ischemia. *J. Cereb. Blood Flow Metab*. 26:1354–1365.
20. Yin, W., G. Cao, M.J. Johnnides, A.P. Signore, Y. Luo, R.W. Hickey, and J. Chen. 2006. TAT-mediated delivery of Bcl-xL protein is neuroprotective against neonatal hypoxic-ischemic brain injury via inhibition of caspases and AIF. *Neurobiol. Dis*. 21:358–371.
21. Zhu, C., L. Qiu, X. Wang, U. Hallin, C. Cande, G. Kroemer, H. Hagberg, and K. Blomgren. 2003. Involvement of apoptosis-inducing factor in neuronal death after hypoxia-ischemia in the neonatal rat brain. *J. Neurochem*. 86:306–317.
22. Zhu, C., X. Wang, Z. Huang, L. Qiu, F. Xu, N. Vahsen, M. Nilsson, P.S. Eriksson, H. Hagberg, C. Culmsee, et al. 2007. Apoptosis-inducing factor is a major contributor to neuronal loss induced by neonatal cerebral hypoxia-ischemia. *Cell Death Differ*. 14:775–784.
23. Bano, D., K.W. Young, C.J. Guerin, R. Lefeuvre, N.J. Rothwell, L. Naldini, R. Rizzuto, E. Carafoli, and P. Nicotera. 2005. Cleavage of the plasma membrane Na+/Ca2+ exchanger in excitotoxicity. *Cell*. 120:275–285.
24. Klein, J.A., C.M. Longo-Guess, M.P. Rossmann, K.L. Seburn, R.E. Hurd, W.N. Frankel, R.T. Bronson, and S.L. Ackerman. 2002. The harlequin mouse mutation downregulates apoptosis-inducing factor. *Nature*. 419:367–374.
25. Zhu, C., X. Wang, F. Xu, B.A. Bahr, M. Shibata, Y. Uchiyama, H. Hagberg, and K. Blomgren. 2005. The influence of age on apoptotic and other mechanisms of cell death after cerebral hypoxia-ischemia. *Cell Death Differ*. 12:162–176.
26. Ye, H., C. Cande, N.C. Stephanou, S. Jiang, S. Gurbuxani, N. Larochette, E. Daugas, C. Garrido, G. Kroemer, and H. Wu. 2002. DNA binding is required for the apoptogenic action of apoptosis inducing factor. *Nat. Struct. Biol*. 9:680–684.
27. Zhu, C., F. Xu, X. Wang, M. Shibata, Y. Uchiyama, K. Blomgren, and H. Hagberg. 2006. Different apoptotic mechanisms are activated in male and female brains after neonatal hypoxia-ischaemia. *J. Neurochem*. 96:1016–1027.
28. Wang, X., J.O. Karlsson, C. Zhu, B.A. Bahr, H. Hagberg, and K. Blomgren. 2001. Caspase-3 activation after neonatal rat cerebral hypoxia-ischemia. *Biol. Neonate*. 79:172–179.
29. Wang, X., C. Zhu, X. Wang, J.G. Gerwien, A. Schrattenholz, M. Sandberg, M. Leist, and K. Blomgren. 2004. The nonerythropoietic asialoerythropoietin protects against neonatal hypoxia-ischemia as potently as erythropoietin. *J. Neurochem*. 91:900–910.
30. Susin, S.A., H.K. Lorenzo, N. Zamzami, I. Marzo, B.E. Snow, G.M. Brothers, J. Mangion, E. Jacotot, P. Costantini, M. Loeffler, et al. 1999. Molecular characterization of mitochondrial apoptosis-inducing factor. *Nature*. 397:441–446.